PERGAMON

Available online at www.sciencedirect.com
SCIENCE DIRECT®

Corrosion Science 45 (2003) 2577–2595

CORROSION SCIENCE

www.elsevier.com/locate/corsci

Comparative study in chemistry of microbially and electrochemically induced pitting of 316L stainless steel

X. Shi [a,b], R. Avci [c,d], M. Geiser [a,e], Z. Lewandowski [a,f,*]

[a] *Center for Biofilm Engineering, Montana State University, Bozeman, MT 59717, USA*
[b] *Department of Mechanical and Industrial Engineering, Montana State University, Bozeman, MT 59717, USA*
[c] *Department of Physics, Montana State University, Bozeman, MT 59717, USA*
[d] *Image and Chemical Analysis Laboratory, Montana State University, Bozeman, MT 59717, USA*
[e] *Department of Chemical Engineering, Montana State University, Bozeman, MT 59717, USA*
[f] *Department of Civil Engineering, Montana State University, Bozeman, MT 59717, USA*

Received 26 November 2002; accepted 4 March 2003

Abstract

Ennoblement of stainless steel (SS) by microbially deposited manganese oxides can lead to pitting corrosion at low chloride concentrations, causing unexpected material failures. We exposed 316L SS to manganese oxidizing bacteria *Leptothrix discophora* under well-defined laboratory conditions, and then placed the ennobled coupons in a 0.5 M sodium chloride solution until pitting developed. Using time-of-flight secondary ion mass spectroscopy we demonstrated that the pits and their immediate vicinity associated with microbial influenced corrosion had different chemical signatures than those associated with electrochemically induced pitting, suggesting a possibility that the microorganisms were directly involved in pit initiation. Based on the differences in the chemical signatures we were able to distinguish the microbially induced pits from those induced by anodic polarization.

Keywords: Pitting; Type 316L stainless steel; Pit chemistry; MIC; *Leptothrix discophora*; Ennoblement

* Corresponding author. Tel.: +1-406-994-5915; fax: +1-406-994-6098.
E-mail address: zl@erc.montana.edu (Z. Lewandowski).

0010-938X/$ - see front matter
doi:10.1016/S0010-938X(03)00079-9

1. Introduction

Current conceptual models concur that there are three stages in the pitting corrosion: initiation, metastable pitting, and active pitting [1–5]. However, the exact mechanisms of pit initiation are difficult to define and thus disputable. For stainless steels (SS), it is agreed upon that manganese sulfide inclusions play a critical role in pit initiation. Recently, Ryan et al. [6] demonstrated that pitting was likely to be "triggered" in chromium-depleted zones formed around MnS particles on the 316F SS surface. We have examined the possible involvement of manganese oxidizing microorganisms in pit initiation on water immersed 316L SS.

When microorganisms are involved in corrosion of metals, the situation is more complicated than it is in an abiotic environment because microorganisms not only modify the near-surface environmental chemistry via microbial metabolism but also may interfere with electrochemical processes occurring at the metal–environment interface. For microbially influenced corrosion (MIC), segregation of elements was reported in specific areas susceptible to pitting, such as grain boundaries on alloy surfaces [7,8]. This effect is similar to the corrosion process, "dealloying", during which the metal is disintegrated by the selective dissolution of its most electrochemically active elements, which leads to the formation of "a nanoporous sponge composed almost entirely of the more noble alloy constituents" [9]. However, for MIC-associated pitting, instead of active it were the electrochemically noble elements, such as chromium in SS materials, were often depleted in the sensitized areas, which may have resulted in preferential anodic dissolution of the alloys [8,10]. This mechanism is well illustrated by (1) microbially assisted depletion of nickel in 90/10 and 70/30 copper–nickel in seawater [11] and (2) significant depletion of Cr and Fe relative to Ni at the grain boundaries of the oxide film on an unpolished 316L SS, which was promoted by the bacterial colonization [12].

Some microorganisms can be detrimental to the integrity of the passive oxide film, and facilitate the local depassivation of the protective layer, therefore promoting ingress of corrosive agents such as the chloride ion. These corrosion mechanisms are of interest to both biofilm and corrosion researchers. However, due to the variety of microorganisms colonizing metal surfaces, and various environmental conditions that may obscure the results, the mechanism of MIC-associated pitting is difficult to investigate, and it may differ for different microorganisms and different environmental conditions. Regardless of the microbial diversity and other uncertainties, there are at least three possible mechanisms by which microbial metabolic reactions can interfere with the electrochemical reactions when the microorganisms colonize metal surfaces:

The first mechanism is related to the heterogeneous distribution of biomass in biofilms. It is well known that biofilms are heterogeneous and modify the near-surface chemical and physical conditions, like decreasing the concentration of oxygen or affecting the distribution of flow velocity [13]. By consuming or generating substances in biofilms, microorganisms cause concentration gradients of components important for their metabolism, which are also important electrochemical reactants, such as oxygen and protons. Since metabolic activity in biofilms is not uniformly

distributed over the colonized surfaces, concentration profiles are formed both vertically and horizontally, and may lead to differential concentration cells [14].

The second mechanism is related the dissolved substances that the microorganisms consume or generate near metal surfaces [15]. In these processes the microorganisms actively use the substrates of electrochemical reaction, like oxygen, and produce other substances that may be used in electrochemical reactions, like hydrogen peroxide. Such changes in near-surface chemistry have an obvious effect on electrochemical reactions related to corrosion.

The third mechanism is related to solid substances the microorganisms deposit, or dissolve, near metal surfaces. It has been demonstrated that the microorganisms deposit inorganic materials on the metal surface or selectively remove alloying elements from the metal substratum, in processes collectively referred to as *biomineralization* [16]. Microbially deposited minerals remain in thermodynamic equilibrium with dissolved substances, and, since the deposits are in electrical contact with the metal, the position of this equilibrium affects the potential of the metal. These shifts in potential may raise the open circuit potential (OCP) of the passive metals near the pitting potential [17,18], and thus add to its susceptibility to pitting corrosion. It is interesting to note that the inorganic deposits not only influence the thermodynamics of the processes related to galvanic corrosion [19], but also modify paths of electron transfer in these processes by linking the corrosion and microbial redox reactions [20].

In conclusion, the synergism of the metal–microorganism interactions usually increases the risk of pitting corrosion, initiates pits, or promotes the propagation of pits.

MIC has been widely implicated in the pervasive material failure of water-immersed SS structures [21–27]. For example, it is expected that 316L SS should not pit in natural waters, even at elevated chloride concentrations [3]. However, cases have been reported of 316L SS failure in natural waters, possibly because of microbial activities. For example, Korin [21] observed the failure of 3-mm thick 316L SS pipes partially filled with well water containing about 200 ppm chloride after four months, where large amounts of manganese and iron were found in the deposits, and both manganese oxidizing bacteria (MOB) and iron oxidizing bacteria (IOB) were identified. Also, Felder and Stein [27] exposed welded 316L SS pipes to a raw water containing 500–600 ppm chloride for four years under various flow conditions, observed bacterial colonization and pitting, and suggested the mechanism of pitting as a result of synergistic effects of metabolic activity of aerobic IOB and anaerobic sulfate reducing bacteria (SRB). Such cases of material failure attract attention to the effect of microorganisms attached to the metal surfaces as possible mediators in the corrosion processes involved.

In the authors' laboratory, the ennoblement of 316L SS by microbially deposited manganese oxides has been systematically explored from a variety of aspects. Presence and activities of MOB can be destructive to the material integrity by causing pitting corrosion at low chloride concentrations. As an undisputable result of bacterial colonization, the increase in OCP of water-immersed 316L SS by about 500 mV is observed, which is also associated with an increase in cathodic current

density by more than two orders of magnitude upon mild polarization [18]. When raised high enough, the elevated OCP may increase the risk of localized corrosion by reaching the critical pitting potential of SS materials.

Searching for the mechanism of ennoblement, Dickinson et al. [18,28] exposed 316L SS coupons to a fresh river, and found distinctive annular deposits comprised of Mn-rich rings 10–20 μm in diameter and filamentous-sheathed cells characteristic of manganese- and iron-oxidizing bacteria (MIOB) within the 3–4 μm diameter central void. 316L SS coupons either coated with MnO_2 paste [18] or exposed to a batch culture of MOB, *Leptothrix discophora* SP-6 [30], both exhibited the ennoblement of OCP and similar electrochemical properties. With the experimental evidence gathered, Dickinson et al. concluded that microbially deposited manganese dioxide was responsible for the observed electrochemical behavior of the *ennobled SS* coupons [18], and proposed a mechanism of pit formation by MIOB as follows [28]: "Ennobled potential due to cathodic MnO_2 depolarization, coupled with diminished redox potential caused by microbial respiration, increases the interfacial potential difference within the rings to a value exceeding the critical pitting potential." Both Dickinson et al. [28] and Linhardt [29] suggested mechanisms explaining ennoblement of SS materials as a result of microbially deposited manganese oxides.

Olesen et al. [31,32] used X-ray photoelectron spectroscopy (XPS) to determine the chemical composition of microbial deposits on ennobled 316L SS and verified the hypothetical mechanism of ennoblement proposed by Dickinson et al. [28] and Linhardt [29]. In addition, Olesen et al. [31,32] demonstrated that MnOOH was an intermediate product of electrochemical reduction of MnO_2 to Mn^{2+} and thus modified the ennoblement mechanism. In view of these results, Shi et al. [33] used the time-of-flight secondary ion mass spectroscopy (ToF-SIMS) to analyze microbial deposits on 316L SS coupons ennobled to various extents, and found that MnOOH was also an intermediate product in the microbial oxidation pathway of Mn^{2+} to MnO_2. The combined results of these studies suggest that while the microbially deposited manganese oxides are electrochemically reduced to divalent manganese, the divalent manganese can be microbially reoxidized by MOB. Such perpetual oxidation–reduction–oxidation of manganese leads to formation of recyclable cathodic reactant, and aggravates the risk of localized corrosive attack. According to this scenario, the cathodic reactants, MnOOH and MnO_2, are renewable through the manganese cycling, and their supply is not limited by thermodynamic activity or by mass transport because they are in solid state and are in electrical contact with the metal surface. Alternative pathways of electron transfer in this mechanism have been also suggested. Ruppel et al. [34] argue that chemical as well as biological reoxidation of Mn^{2+} to MnO_2 probably takes place in natural marine biofilms.

Ennoblement of SS and other passive metals can lead to localized corrosion. Working on this premise, Geiser et al. [35,36] investigated the role of MOB in pit initiation by exposing 316L SS coupons to a batch culture of *L. discophora* SP-6 in a mineral–salt–pyruvate–vitamin medium containing divalent manganese. The ennobled coupons were cleaned by mechanically removing the biofilm from the surface, and then immersed in a 0.2 M sodium chloride solution until the corrosion pits developed. At different times of exposure to the chloride solution, the surface of SS

coupons was examined using scanning electron microscopy (SEM) and atomic force microscopy (AFM). The coupons exposed to the microorganisms, but not yet treated with the chloride, had odd indentations on the surface, suggesting that the microorganisms were directly involved in the pit initiation. Geiser et al. [35] also demonstrated that the pits formed in the presence of microorganisms had distinctly different morphologies than those generated by electrochemical polarization of 316L in an abiotic solution, documenting that the pits formed in the microbially ennobled coupons had the size, shape, and aspect ratio very similar to that of the MOB colonizing the surface. Based on these results, Geiser et al. [35] hypothesized that in the MIC-associated pitting pits were initiated exactly at the sites where the bacteria were attached.

If the pits initiated in the presence and absence of microorganisms are indeed different, their chemical composition should be different. Thus far, evidence attributing localized corrosion to microbial activities has been indirect, usually based on the analysis of deposits accumulated on the metal surface long after the corrosion had been initiated [37]. However, the results shown by Geiser et al. imply that chemical evidences of microbially induced changes of the passive layer may be detectable. In particular, the chemistry within and outside the pits should be different and depend on whether the pits were generated in the presence or absence of microorganisms. Therefore, we hypothesize here that the chemistry of SS surfaces that was subjected to microbially induced pitting should be different from the chemistry of the same material subjected to pitting corrosion in an abiotic environment.

Testing the presented hypothesis calls for surface analysis tools of high sensitivity coupled with capability of chemical imaging. Traditional analytical techniques of metal surfaces, such as auger electron spectroscopy (AES) and XPS [12,38], have been successfully applied to characterize the chemical composition of the SS passive film and its change as a result of being exposed to different environments. However, determining surface chemistry within the pits on the SS surface requires more sensitive analytical techniques that can collect chemical information at micron scale with reasonable accuracy. XPS does not have adequate spatial resolution to provide such information, and AES is not favored since the data from the insulated areas (microbial minerals) are not reliable due to sample charging. Therefore, the instrument of choice was ToF-SIMS, which offers adequate chemical imaging capability and sensitivity that are able to determine the chemical composition of corrosion pits and their immediate vicinity on 316L SS.

The goal of this work was to determine the chemical features distinguishing the microbially induced corrosion pitting from the *electrochemically induced pitting* on 316L SS. To reach this goal, we run two sets of experiments:

(1) Exposed 316L SS coupons to a pure culture of *L. discophora* (to grow biofilms on the surface) until the coupons were ennobled to more than +300 mV_{SCE}, cleaned the biofilms from the coupon surfaces, and then placed the ennobled coupons in a 0.5 M sodium chloride solution until they were pitted.
(2) Exposed non-ennobled 316L SS coupons to a 0.5 M sodium chloride solution and applied +300 mV_{SCE} to the coupons until they were pitted.

Using ToF-SIMS, we determined surface chemistry of non-ennobled 316L SS, ennobled 316L SS with biofilms removed, and 316L SS after microbially or electrochemically induced pitting, respectively. The secondary ion mass spectra were analyzed in terms of relative intensities of different elements including manganese, iron, and chromium, and in terms of intensity ratios characteristic of their oxidation states. We also imaged the spatial distribution of different alloying elements on the metal surface at micron scale to illustrate the difference between the chemistries on surfaces that were exposed to microbially and electrochemically induced pitting. Location of the pits has been assigned using the elemental distribution of Cr^+ ions, i.e., the chromium-depleted zones mark the location of the pits, which is backed by the findings of Ryan et al. [6].

2. Materials and methods

2.1. Metal samples

316L SS corrosion coupons, each 1.6 cm in diameter, were cut from larger sheets provided by Metal Samples, Inc. (Munford, AL). Table 1 lists the nominal elemental composition (wt.%) of 316L SS coupons as provided by the vendor. The coupons were polished following the procedures described in our previous publication [33] to the 0.05-μm level and were sonicated, first in acetone, then in 95% ethanol, for 5 min in each solvent. The coupons were then mounted in polycarbonate holders using a 100% silicone sealant (from Ace Hardware Co.) and were electrically connected by fixing conductive springs to the unexposed side so that the monitoring of OCP was made possible. Prior to use, the coupons were left in contact with atmospheric air for 24 h to form a protective layer of metal oxides on the surface. Such coupons are referred to as intact *SS* coupons (or intact *SS* surfaces) in the text.

2.2. Laboratory ennoblement experiment

The reactor was a polycarbonate batch cylinder reactor, 10.2 cm tall and 11.1 cm in diameter, the same as that used by our previous work [33]. Eight polished coupons were mounted face down through holes in the lid of the reactor. Glass tubes were mounted in the reactor to aerate the growth medium and aseptic air vents were attached to them to prevent any possible contamination. A magnetic stir bar, placed at the bottom of the reactor, provided stirring. The reactor was then sealed with silicon gel and autoclaved on the dry setting (depressurization method) at 123 °C and 1.2 atm for 30 min. After the reactor was cooled down to room temperature, a

Table 1
The nominal elemental composition (wt.%) of 316L SS coupons

Fe	Cr	Ni	Mo	Mn	Si	P	N	C	S
Balanced	16.19	10.19	2.10	1.71	0.39	0.034	0.03	0.017	0.001

sterilized SCE reference electrode was mounted to the reactor. The coupon assembly and the SCE were electrically connected through a salt bridge containing 1% agar and 1 mM Na_2SO_4, and both of them were connected to a computer via a Hewlett Packard 34970A Data Acquisition/Switch Unit (a 20-channel Armature multiplexer) to monitor the OCPs of the coupons. Prior to inoculating the reactor with *L. discophora*, the coupons were immersed in the culture medium for 48 h to make sure that the OCPs were stabilized. After inoculation, the reactor was operated until the potentials of the coupons exceeded +350 mV_{SCE}, and remained stable around that value, which, by our experience, indicated that the ennoblement of the coupons was fully achieved and microbially deposited manganese oxides on the SS surface were mainly in the form of manganese dioxide. Using these experimental procedures, it took about 80 h to ennoble the coupons.

The MOB, *L. discophora* SP-6, were obtained from American Type Culture Collection (ATCC no. 51168) and stored at −70 °C. To inoculate the reactor, we poured 150 ml of mineral–salt–pyruvate–vitamin (MSPV) medium (ATCC no. 1917) into a sterile 250-ml Erlenmeyer flask already holding the stock culture of the bacteria. The flask was placed on a shaker for two days, and then the culture broth was aseptically mixed with 600 ml of the sterile medium and added to the reactor.

For laboratory exposure of 316L SS to *L. discophora*, we prepared 1 l of the MSPV medium, of which 1 ml of filter-sterilized vitamin solution and 5 ml of filter-sterilized 20% sodium pyruvate solution were aseptically added after the rest of nutrient solution was autoclaved on the liquid setting at 123 °C and 1.2 atm for 25 min and cooled to room temperature. We also aseptically added 4 ml of filter-sterilized 50-mM manganese sulfate solution to the cooled growth medium. All chemicals were from Fisher Scientific.

2.3. Pitting experiments

To investigate the *microbially induced pitting*, we used 316L SS coupons ennobled by *L. discophora* to over +350 mV_{SCE}. After ennoblement, the metal surface was cleaned carefully with distilled water and paper tissue such that enough microbially deposited minerals were kept on the surface to maintain the potential at over +300 mV_{SCE}. Such a surface is referred to as ennobled SS surface in the text. Then, we exposed the SS coupons to a 0.5 M sodium chloride solution and monitored their OCPs to determine the progress of pitting. The process continued for seven days and pits were developed. Such treatment is referred to as MIC-associated pitting or microbially induced pitting in the text.

To investigate the electrochemically induced pitting, anodic polarization of 316L SS coupons was performed using a flat type three-electrode electrochemical cell, with an SCE reference electrode and two high-density graphite counter-electrodes. An EG&G Potentiostat/Galvanostat model 273A was employed, which was interfaced to and controlled by a computer using the 352 SoftCorr III corrosion measurement software by EG&G Princeton Applied Research. We applied a potential of +300 mV_{SCE} to the working electrode, namely, the 316L SS coupon exposed to a 0.5 M

Table 2
Summary of various nomenclatures used throughout the text and their description

Nomenclature	Description
Intact SS surface	Refers to the surfaces associated with as-received SS coupons polished and cleaned as described in the text before being subjected to microbial or electrochemical treatment
Ennobled SS surface	Refers to the surfaces of polished SS coupons that are first microbially ennobled to +350 mV_{SCE} (by *L. discophora*), and then biofilms are removed from the metal surface but still maintain an OCP not lower than +300 mV_{SCE}
Microbially induced pitting	Refers to the pits formed on polished SS coupons by further exposing ennobled SS surface to a 0.5 M NaCl solution for seven days
Electrochemically induced pitting	Refers to pits formed on polished SS coupons that are exposed to a 0.5 M NaCl solution for 4 h, while +300 mV_{SCE} are applied to them externally (also known as anodic polarization)

sodium chloride solution. The process continued for 4 h and pits were developed. Such treatment is referred to as electrochemically induced pitting in the text.

In what follows the nomenclatures such as intact SS, ennobled SS, microbially induced pitting, and electrochemically induced pitting of 316L SS coupons are frequently used. Summary and description of these terms are listed in Table 2 for convenience.

2.4. Surface analysis

A major technical difficulty associated with the experiments was to find exactly the same locations on the 316L SS surface before and after microbial colonization and/or pitting. Only then the chemical changes in the metal surface could be attributed to the microbial colonization and/or pitting. To accomplish this task we marked small identifiable squares (180×180 μm^2) near the center of the intact SS surface using a focused ToF-SIMS Ga^+ ion beam and the programmable rastering routine. The ion milling for pattern formation was performed for seven minutes at $\sim$1.2 nA ion current and $\sim$22 keV impact energy, which produced trenches approximately 100 nm deep on the metal surface. With a Digital Instruments Dimension 3100 scanning probe microscope in contact mode, we employed AFM imaging to register the topography of the surface within these squares.

For the analysis of the ennobled SS coupons, we gently cleaned the surface using distilled water and paper tissue such that most biofilms were removed and enough microbially deposited minerals were kept on the metal surface. For the analysis of the SS coupons after microbially induced pitting or electrochemically induced pitting, we removed them from the chloride solution, rinsed the surface using distilled water to remove any dissolvable substances. All the SS coupons were then mechanically removed from the holders, air-dried and kept in separate airtight containers for up to 24 h prior to SIMS analysis to ensure dryness.

Four iron oxides were used as standards to collect SIMS reference spectra. These are FeO (99.9%, Aldrich), Fe_2O_3 (99.999%, ACROS), Fe_3O_4 (Lab. grade, Fisher),

and FeOOH (99.8%, Strem). We prepared the standards for SIMS analysis by gently pressing the powdered compounds into a piece of soft indium foil (Alfa, ESAR), using clean glass slides to ensure that the surface to be analyzed was flat. As a result, the sample spectra included a peak from indium, but this did not interfere with any peaks of importance for this study.

ToF-SIMS analyses of the coupons and oxide standards were conducted using a Phi-Evans TRIFT I mass spectrometer. The working principle of such system can be found in advanced texts on surface analytical techniques [39–41] and in our earlier publication [33]. Basically, ToF-SIMS is an imaging mass spectroscopy analysis that allows obtaining high-resolution mass spectra and micron-scale chemical maps. The analyses were accomplished by rastering a focused primary ion beam across the surface of interest while collecting secondary ion mass spectroscopy at each point. We used a pulsed gallium liquid metal ion gun (LMIG) fired at 25 keV primary energy, with a 10-kHz repetition rate, as the primary ion source. A multi-stop time-to-digital converter (TDC) recorded the time-of-flight of the ion fragments with a 138-ps precision. The LMIG pulse width was kept <14 ns while the raster size of the beam varied from 80×80 μm^2 to 240×240 μm^2, combination of all of which yielded ~1 μm spatial resolution while simultaneously detecting ion fragments with $\sim m/\Delta m \sim 1500$ mass resolution. In all of the ToF-SIMS acquisitions we stayed within the limit of static SIMS requirements, which means the primary ion dose remained below 10^{13} ions per cm^2. A beam of low-energy (<20 eV) electrons was fired intermittently to prevent charging of the sample. The data acquisition and analysis were done using both DOS and Win-Cadence ToF-SIMS software (Physical Electronics).

The analysis and comparison of surface chemistry of user-specified zones were made possible by utilizing the region-of-interest (ROI) feature of ToF-SIMS. The raw data acquisition of ToF-SIMS stores a complete mass spectrum for each of the 256×256 pixels uniformly distributed through the area of detection. Retrospective analysis of the raw SIMS data files enabled us to obtain chemical maps of the specific ion fragments and to obtain mass spectral data from the specific zones of our interest. The main objective of imaging SIMS analysis was to demonstrate that chemical differences between the pits and their immediate vicinity could be observed and the differences depend on the pitting mechanism, which in turn shed light on the fundamental nature of the mechanisms.

3. Results and discussion

3.1. Chemical mapping and morphology of the intact 316L SS surface

To prepare the reference, we first created a few grid patterns (180×180 μm^2) on each intact SS surface through ion milling by ToF-SIMS. Then, we collected the SIMS spectra of every marked area (240×240 μm^2) on the intact SS surface and from the data file we generated distribution maps of Mn^+, Fe^+(MnH^+), FeH^+, Cr^+, and CrH^+ for each area. Fig. 1 shows the distribution maps for a typical marked area. As illustrated in our previous publication [42], the secondary ion signals, Fe^+

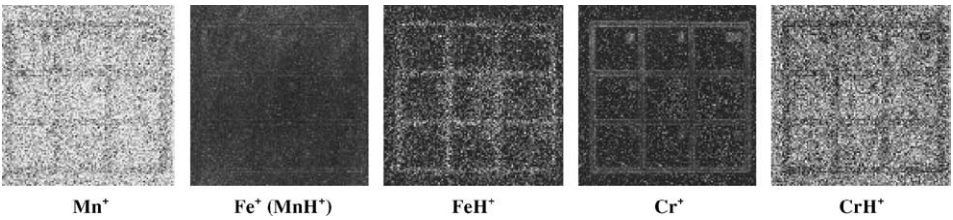

Fig. 1. ToF-SIMS images showing the distribution of secondary ions: Mn^+, $Fe^+(MnH^+)$, FeH^+, Cr^+, and CrH^+. Data collected from a 240×240 μm^2 area on an intact SS coupon. Numbers were etched at the higher left corner of each grid in the square (Fig. 2) and were clearly identifiable in the map of total secondary ions (0–1000 amu). The entire square was 180×180 μm^2. Secondary ion intensity is proportional to darkness of the image (the blacker it is, the more counts per pixel it has).

and MnH^+ at about 56 amu, overlap and cannot be resolved without numerical analysis. From Fig. 1, we can see that manganese, iron, and chromium are uniformly distributed on the intact SS surface. To image the topography of the surface before subjecting it to any biological or electrochemical process, we recorded the preexisting surface morphology using AFM. Fig. 2 further confirms that the marked areas on the intact SS surface are free of flaws.

3.2. Chemical mapping of the 316L SS surface after electrochemically and microbially induced pitting

We observed that simple immersing 316L in 0.5 M sodium chloride did not initiate pitting. However, when we polarized 316L SS +300 mV_{SCE} to increase its vulnera-

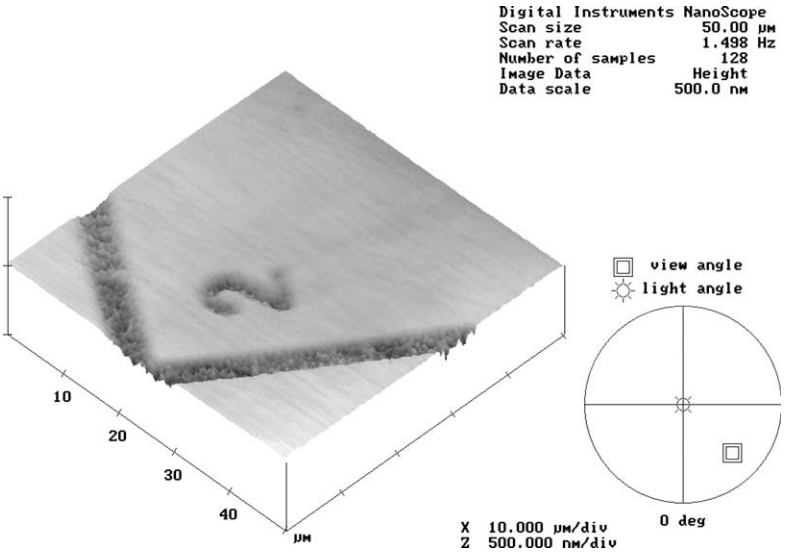

Fig. 2. A 50×50 μm^2 AFM image of a section of a square etched on an intact SS surface (Fig. 1) by ion milling. Notice the number '2' etched in the lower left corner for identification.

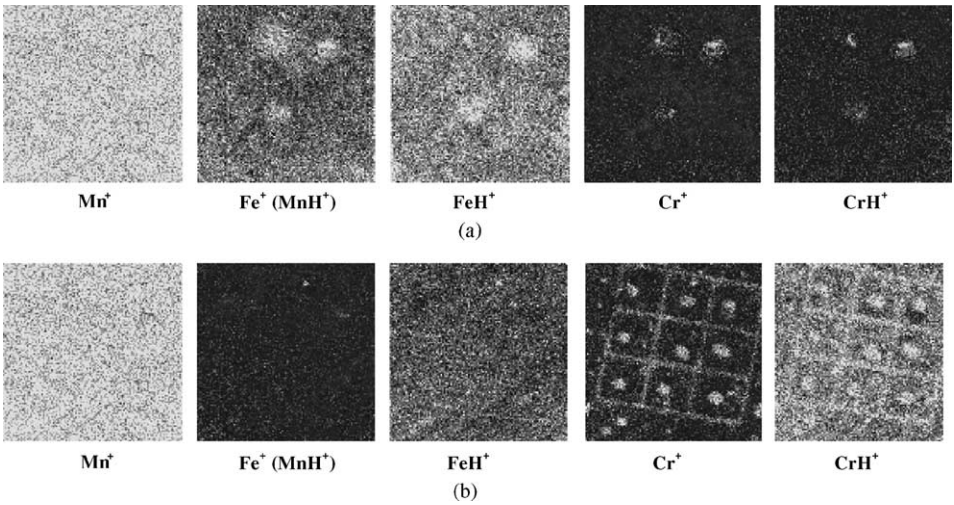

Fig. 3. ToF-SIMS images showing the distribution of secondary ions: Mn^+, $Fe^+(MnH^+)$, FeH^+, Cr^+, and CrH^+. Data collected from a 240×240 μm^2 area on a 316L SS coupon subjected to (a) electrochemically induced pitting; (b) microbially induced pitting. In all images the secondary ion intensity is proportional to the darkness of the scale (the blacker, the stronger). In both figures the white spots in Cr maps indicate the pitted zones.

bility, significant pitting was observed during the 4-h exposure, as indicated by the fluctuations of OCP. Unfortunately, the grid patterns that were well visible on the intact SS surfaces (Fig. 1) could not be located on the coupon surfaces after electrochemically induced pitting. Hence, we randomly chose an area of 240×240 μm^2 located at the approximate site on the surface as the marked area. We collected the SIMS spectra of a few marked areas on each SS surface after electrochemically induced pitting and generated distribution maps of Mn^+, $Fe^+(MnH^+)$, FeH^+, Cr^+, and CrH^+ for each area. Fig. 3a shows the chemical maps for an example of such area.

316L SS coupons were exposed to a batch culture of *L. discophora* until their OCPs exceeded +350 mV_{SCE}. After removing the biofilms from the metal surface, the OCP of the ennobled coupons decreased slightly, but still was not lower than +300 mV_{SCE}. [1] During the seven-day exposure of the ennobled SS coupons to 0.5 M Cl^-, metastable pitting was observed and the OCP was unstable, jumping between 0 and +180 mV_{SCE}. The grid patterns were still visible on the coupon surfaces after microbially induced pitting, even though the marked numbers were not. We chose a 240×240 μm^2 area containing the pattern as the marked area and its location was almost the same as the one used for control. We collected the SIMS spectra of a few marked areas on each SS surface after microbially induced pitting and generated

[1] The OCP decrease may be explained by the removal of some of the surface manganese dioxide within the biofilms while the remaining minerals left on the surface, most likely a mixture of manganese dioxide and manganese oxyhydroxide, maintained the OCP over +300 mV_{SCE}.

distribution maps of Mn^+, $Fe^+(MnH^+)$, FeH^+, Cr^+, and CrH^+ for each area. Fig. 3b shows the chemical maps for an example of such area. We cannot explain the regularity of the white spots in the Cr^+ map, i.e., chromium-depleted zones (hence the pits), which formed in the middle of every grid and might be somehow related to the creation of the grid patterns via ion milling.

For both types of pitting corrosion, we identified the chromium-depleted zones as pits. For the SS surface subjected to electrochemically induced pitting, we observed that iron was depleted within the pits as compared to the zones surrounding the pits (Fig. 3a). For the SS surface subjected to microbially induced pitting, however, the difference in iron intensity between pits and their immediate vicinity was less apparent. For both types of pitting corrosion, the intensity difference in manganese between pits and their immediate vicinity were below the level of detection, possibly because the manganese signals were much weaker than iron and chromium to begin with. All these conclusions are based on the comparison of the relative signal intensities of secondary ions detected by ToF-SIMS.

To further illustrate the chemistry changes of SS surface subjected to different treatments, we collected the secondary ion mass spectra from a 60×60 μm^2 area of 316L SS surface subjected to ennoblement, microbially induced pitting, and electrochemically induced pitting (see Table 2 for details), respectively. The Mn^+ and Cr^+ distribution maps corresponding to each sample preparation are shown in Fig. 4 for comparison.

From Fig. 4a, it is clear that on ennobled SS surface Mn^+ signals are enriched in some zones where Cr^+ signals are correspondingly depleted. There are also zones where Cr^+ signals are depleted but Mn^+ signals are not correspondingly enriched. Hence, we hypothesized that the chromium-depleted zones either mark the location of coverage by manganese-enriched microbial deposits, or mark the sites of pit initiation. As indicated in Fig. 4b, the manganese-enriched deposits were consumed by the subsequent pitting during which the ennobled SS surface was further exposed to chloride ions.

Fig. 4b and c show that after both types of pitting corrosion, the depletion or enrichment of manganese in certain zones on the SS surface, if any, is not apparent. The Cr^+ map in Fig. 4b suggests that pitting was developed after exposing the ennobled SS surface to chloride solution, which was distinguished by the characteristically oval zones depleted in chromium. On the contrary, Fig. 4c shows that the

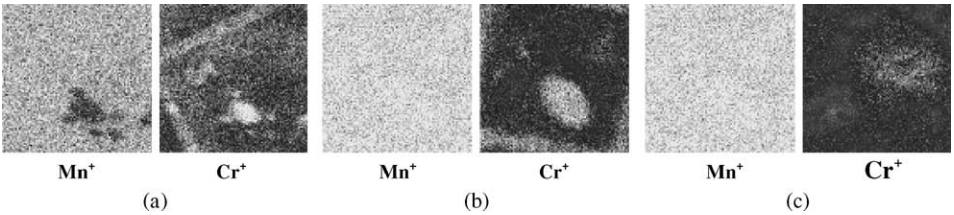

Fig. 4. ToF-SIMS images showing the distribution of secondary ions: Mn^+ and Cr^+. Data collected from a 60×60 μm^2 area on a 316L SS coupon subjected to (a) ennoblement, (b) microbially induced pitting, and (c) electrochemically induced pitting.

Table 3
The relative intensity of selected secondary ions in the positive SIMS spectra for a 316L SS surface subjected to various treatments

	Mn^+	$Fe^+(MnH^+)$	FeH^+	Cr^+	CrH^+	Sum
Intact SS surface	2.4	44.9	13.9	31.4	7.4	100
Ennobled SS surface	6.0	50.7	17.2	20.8	5.3	100
Zones surrounding MIC-associated pits	1.7	44.4	13.4	32.7	7.7	100
MIC-associated pits	1.8	60.9	18.2	15.1	3.9	100
Electrochemically induced pits	0.7	13.6	4.1	66.2	15.4	100
Zones surrounding electrochemically induced pits	0.6	11.8	3.4	69.1	15.1	100

The sum total area under the selected peaks (count of secondary ions) is normalized to 100%. The numbers in each entry represents the percentage peak area, instead of absolute concentration. For example, for the "intact SS surface", the Cr^+ ions account for 31.4% of the total counts of secondary ions listed above.

chromium depletion within the pits is less significant for electrochemically induced pitting. Though the differences in the chromium depletion are revealing, all chemical changes must be taken into account to illustrate the difference in pitting mechanisms in the presence or absence of microorganisms. In what follows we compare the changes in the elemental composition and the oxidation state of the passive films subjected to the two types of corrosion mechanisms.

3.3. Changes in the elemental composition within the 316L SS surface film

To investigate the mechanisms of microbially and electrochemically induced pitting, we collected the SIMS spectra from several zones on the surface of each SS coupon, including intact SS surface, ennobled SS surface, SS surface subjected to microbially induced pitting, and SS surface subjected to electrochemically induced pitting. For SS surfaces subjected to various treatments, we compared their elemental composition of manganese, iron, and chromium in zones of interest (using the ROI feature of ToF-SIMS). [2] The comparison was performed in terms of percentage intensity, summing up to 100%, of secondary ion counts of interest, and the results are shown in Table 3. These results are further supplemented by comparing the peak areas of Mn^+, Cr^+, and CrH^+ relative to $Fe^+(MnH^+)$ peak area, and the results are shown in Fig. 5.

It is clear that within the intact SS surface, the manganese concentration ($Mn^+ \sim 2.4\%$, Table 3) is much lower than that of iron ($Fe^+ \sim 44.9\%$, Table 3), which is consistent with the elemental composition of 316L SS (Table 1), and therefore, the contribution of MnH^+ to the $Fe^+(MnH^+)$ peak at 56 amu is insignificant.

Results in Table 3 show that within the ennobled SS surface, manganese concentration (indicated by Mn^+) significantly increased from 2.4% to 6.0% and chromium concentration (indicated by Cr^+) decreased from 31.4% to 20.8% whereas iron

[2] Although nickel is present in the bulk of 316L SS (Table 1), its related secondary ion signals were too weak to be clearly defined, indicating nickel concentration in the passive layer is negligible.

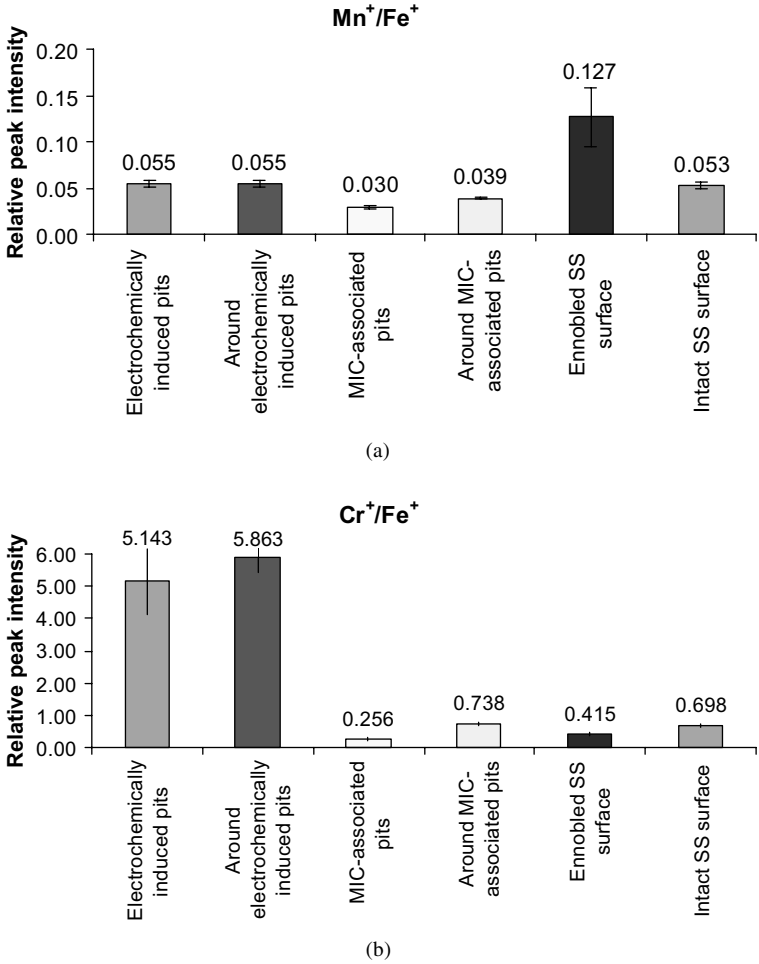

Fig. 5. The relative intensity of (a) Mn^+ and (b) Cr^+ versus the $Fe^+(MnH^+)$ peak in positive SIMS spectra as a function of zones from a SS surface subjected to various treatments, i.e., electrochemically induced pitting, ennoblement, and microbially induced pitting.

concentration (indicated by Fe^+) increased from 44.9% to 50.7%. Fig. 5 shows that after ennoblement the Mn^+/Fe^+ ratio increased by 140% whereas the Cr^+/Fe^+ ratio decreased by 40%. Therefore, we concluded that the relative increase of manganese concentration was mostly due to the deposition of manganese oxides on the metal surface, and the relative increase of iron concentration was most likely due to the decrease of chromium concentration within the passive film. The results show that the microbial colonization of *L. discophora* on 316L SS selectively removed chromium from the metal surface. As chromium is the protective alloying element in the passive film, the material integrity of 316L SS was endangered even before the attack of chloride ions. This supports the finding of Geiser et al. [35,36] that *L. discophora*

caused the odd indentations on 316L SS coupons before they were exposed to the chloride solution.

We explored the mechanism of microbially induced pitting by comparing the chemistry between MIC-associated pits and their immediate vicinity on 316L SS. As opposed to the intact SS surface, there is slight decrease in iron concentration (from 44.9% to 44.4%) as well as slight increase in chromium concentration (from 31.4% to 32.7%) for the immediate vicinity surrounding MIC-associated pits on the metal surface (see Table 3). Within the pits, however, we saw a significant decrease in chromium (from 31.4% to 15.1%) accompanied by an increase in iron concentration (from 44.9% to 60.4%). Fig. 5 shows that the ratios Cr^+/Fe^+ significantly decreased within pits by 63% and slightly increased within their immediate vicinity by 6%, whereas the Mn^+/Fe^+ ratio decreased in both zones by 43% and 26%, respectively. Therefore, we concluded that due to microbial activities and to subsequent pitting progress, chromium was selectively removed within MIC-associated pits while iron was selectively removed within their immediate vicinity. In both zones, manganese was selectively removed (as opposed to iron) from the metal surface, indicating that manganese from the metal as well as divalent manganese from the environment may act as the supply for the manganese-enriched minerals deposited by the MOB.

We also explored electrochemically induced pitting by comparing the chemistry of corrosion pits and their immediate vicinity on 316L SS anodically polarized in chloride solution. From Table 3, it was found that the manganese and iron concentrations decreased significantly (Mn^+: from 2.4% to 0.7%; Fe^+: from 44.9% to 13.6%) while the chromium concentration increased significantly (Cr^+: from 31.4% to 66.2%) within the pits. Similarly, the manganese and iron concentrations decreased significantly (Mn^+: from 2.4% to 0.6%; Fe^+: from 44.9% to 11.8%) while the chromium concentration increased significantly (Cr^+: from 31.4% to 69.1%) for zones surrounding the pits. From Fig. 5, it is clear that for electrochemically induced pits and their immediate vicinity the Mn^+/Fe^+ ratio was maintained the same level as that in the intact surface while the ratios Cr^+/Fe^+ was significantly increased by 637% and 740%, for pits and immediate vicinity, respectively. We concluded that the electrochemically induced pitting caused the disintegration of the passive film of 316L SS, during which the selective dissolution of its electrochemically active elements, iron and manganese, led to the enrichment of its more noble alloy constituent, chromium. This mechanism is similar to the "dealloying" process [8]. The selective dissolution of Fe and Mn was not performed uniformly on the SS surface, and those zones where more Fe and Mn were depleted became more enriched in Cr and thus were more protective to further attack of chloride. This is in accordance with the observation that within the pits the Cr^+/Fe^+ ratio was lower than those of their immediate vicinity.

To summarize, during microbially induced pitting Cr was selectively removed from pitted zones and Fe was selectively removed from zones surrounding the pits on the 316L SS surface, whereas during electrochemically induced pitting Fe and Mn (relative to Cr) was selectively removed from the whole 316L SS surface. Such mechanisms caused significant differences in the surface chemistry between 316L SS

subjected to these two types of pitting corrosion, which can be used to identify the fingerprint of microbially induced pitting.

3.4. Changes in the oxidation state of chromium and iron within the 316L SS surface film

In addition to the changes in the elemental composition within the 316L SS surface film caused by microbial colonization and/or pitting, we also detected the changes in the oxidation state of chromium and iron. As explained in our previous publication [33], SIMS is also capable to identify the oxidation state of minerals using characteristic intensity ratios. In this paper, we used CrH^+/Cr^+ and FeH^+/Fe^+ to identify the changes in oxidation state of chromium and iron, respectively. Any change in the ratios CrH^+/Cr^+ and FeH^+/Fe^+ as a result of a treatment can be attributed a change in the oxidation state of Cr and Fe, respectively. Fig. 6 shows the intensity ratios, CrH^+/Cr^+ and FeH^+/Fe^+, in positive SIMS spectra as a function of zones from a SS surface subjected to various treatments.

As shown in Fig. 6a, the CrH^+/Cr^+ ratio increased slightly from 0.236 to 0.265 after ennoblement, suggesting that the microbial colonization of *L. discophora* on 316L SS not only selectively removed chromium from the metal surface, but also transformed the oxidation state of chromium oxides within the metal surface. This is deduced from the observation that CrH^+/Cr^+ ratio increased from 0.236 to 0.275 within the MIC-associated pits, whereas the oxidation state of chromium in their immediate vicinity remained the same as the intact unexposed SS surface (CrH^+/Cr^+ ratio remained 0.236). Fig. 6a also indicates that oxidation state of chromium, as a result of the electrochemically induced pitting, changed in both zones (within pits and their immediate vicinity). The ratios CrH^+/Cr^+ for the Cr oxide standards are lacking at this stage for a clear identification of the oxidation state of chromium described above, but chromium is most likely transformed or oxidized due to the anodic polarization in chloride solution.

To identify the oxidation state of iron oxides within the SS surface, we determined the ion intensity ratios of FeH^+/Fe^+ for iron oxides, FeO, Fe_2O_3, Fe_3O_4, and FeOOH, as standards, and these ratios in positive SIMS spectra are shown in Fig. 7. Taking into account the chemistry and comparing the standard ratios with the FeH^+/Fe^+ ratios in Fig. 6b the oxidation state of iron oxides on SS surfaces were identified, even though their standard deviations were relatively high. Since the FeH^+/Fe^+ ratio (0.311) was between that of Fe_2O_3(0.330) and Fe_3O_4(0.306), the iron oxides within the intact SS surface were mainly a mixture of Fe_2O_3 and Fe_3O_4. After ennoblement, the iron oxides on the surface were mainly Fe_2O_3.

Based on the FeH^+/Fe^+ ratios, we hypothesized that the iron oxides within the SS surface after microbially induced pitting, both within the pits and their immediate vicinity, were a mixture of Fe_3O_4 and FeOOH, indicating that Fe_2O_3 was transformed by the microbial metabolism of *L. discophora* to FeOOH. On the other hand, we hypothesized that the iron oxides within the SS surface after electrochemically induced pitting were mainly Fe_3O_4 within the pits and FeOOH within their immediate vicinity.

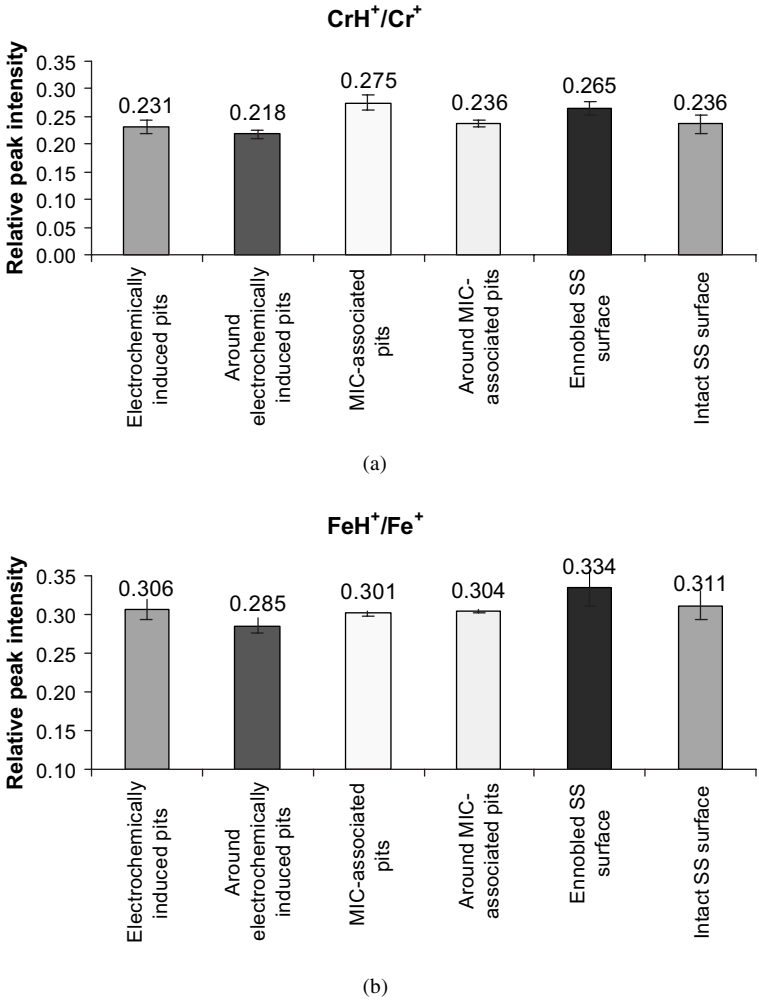

Fig. 6. The intensity ratios, (a) CrH^+/Cr^+, (b) $FeH^+/Fe^+(MnH^+)$, in positive SIMS spectra as a function of zones from a SS surface subjected to various treatments, indicating the changes in the oxidation state of chromium and iron.

4. Conclusions

- Ennoblement process caused by biofilms of *L. discophora* SP-6 on the 316L SS surface under well-defined conditions not only deposits manganese-containing minerals on the metal surface, but also selectively removes chromium and manganese (relative to iron) from the passive layer and changes the oxidation state of chromium and iron oxides within the SS surface by transformation and/or oxidation. Further exposure of the ennobled surface to a 0.5 M chloride solution

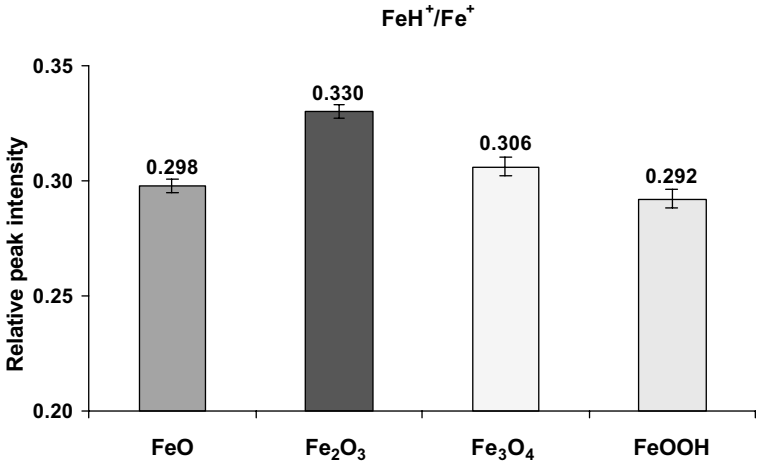

Fig. 7. The intensity ratio FeH^+/Fe^+ in positive SIMS spectra as a function of different iron oxide standards, FeO, Fe_2O_3, Fe_3O_4, and FeOOH.

initiates pitting corrosion by further removing the chromium within the pits while selectively removing the iron from the zones surrounding the pits.

- Pitting corrosion as a result of anodic polarization of 316L SS coupons in a 0.5 M chloride solution disintegrates the passive film by selective dissolution of iron and manganese, causing a relative enrichment of chromium within the whole metal surface. The pitting process transforms and/or oxidizes the chromium and iron oxides both within the pits and their surrounding zones on the 316L SS surface.

Acknowledgements

This work was supported by United States Office of Naval Research, contract number N00014-99-1-0701 and N-00014-02-1-0567, and by Cooperative Agreement EEC-8907039 between the National Science Foundation and Montana State University, Bozeman, MT, USA. We would also like to specially thank the ICAL facility of Montana State University for their help with using the AFM and ToF-SIMS.

References

[1] G.S. Frankel, J. Electrochem. Soc. 145 (6) (1998) 2186.
[2] A.J. Sedriks, Corrosion of SSs, Corrosion Monograph Series, vol. XVIII, second ed., John Wiley & Sons, New York, 1996, p. 437.
[3] Z. Szklarska-Smialowska, Pitting Corrosion of Metals, NACE, Houston, 1986, p. 431.
[4] T. Shibata, T. Takeyama, Corrosion 33 (7) (1977) 243.
[5] N.J. Laycock, R.C. Newman, Corros. Sci. 39 (10/11) (1997) 1771.

[6] M.P. Ryan, D.E. Williams, R.J. Chater, B.M. Hutton, D.S. Mcphail, Nature 415 (2002) 770.
[7] C.R. Das, K.G. Mishra, Biologically Induced Corrosion, NACE, Houston, 1985, p. 114.
[8] S.M. Bruemmer, Mater. Sci. Forum 46 (1989) 309.
[9] J. Erlebacher, M.J. Aziz, A. Karma, N. Dimitrov, K. Sieradzki, Nature 410 (2001) 450.
[10] D. Cubicciotti, G.J. Licina, Mater. Perform. 29 (1) (1990) 72.
[11] B. Little, J. Jacobus, L. Janus, Estuaries 12 (1989) 138.
[12] G.G. Geesey, R.J. Gillis, R. Avci, D. Daly, M. Hamilton, P. Shope, G. Harkin, Corros. Sci. 38 (1) (1996) 73.
[13] S.C. Dexter, G.Y. Gao, Corrosion 44 (10) (1988) 717.
[14] F.L. Roe, Z. Lewandowski, T. Funk, Corrosion 52 (10) (1996) 744.
[15] J.K. Glenn, M.H. Gold, Arch. Biochem. Biophys. 242 (1985) 329.
[16] B.J. Little, P.A. Wagner, Z. Lewandowski, in: Proceeding of Corrosion 1998, Paper no. 294, NACE, Houston, TX, 1998.
[17] I.G. Chamritski, G.R. Burns, B.J. Webster, N.J. Laycock, in: Proceeding of Corrosion 2001, Paper no. 01254, NACE, Houston, TX, 2001.
[18] W.H. Dickinson, F. Caccavo Jr., Z. Lewandowski, Corros. Sci. 38 (8) (1996) 1407.
[19] Z. Lewandowski, W. Dickinson, W. Lee, Water Sci. Technol. 36 (1) (1997) 295.
[20] W.A. Hamilton, Microbially influenced corrosion in the context of metal microorganism interactions, in: L.V. Evans (Ed.), Biofilms: Recent Advances in Their Study and Control, Harwood Academic Publishers, Australia, 2001, pp. 419–434.
[21] G. Korin, Mater. Perform. 15 (7) (1976) 38.
[22] D.H. Pope, D.J. Duquette, A.H. Johannes, P.C. Wayner, Mater. Perform. 23 (4) (1984) 14.
[23] J.G. Stoecker, D.H. Pope, Mater. Perform. 25 (6) (1986) 51.
[24] V. Scotto, G. Alabiso, G. Marcenaro, Bioelectrochem. Bioenerg. 16 (1986) 347.
[25] S.D. Strauss, Power 135 (1991) 50.
[26] G. Korin, Mater. Perform. 33 (4) (1994) 62.
[27] C.M. Felder, A.A. Stein, in: Proceeding of Corrosion 1994, Paper no. 275, NACE, Houston, TX, 1994.
[28] W.H. Dickinson, Z. Lewandowski, Biofouling 10 (13) (1996) 79.
[29] P. Linhardt, Mater. Sci. Forum 289–292 (1998) 1267.
[30] W.H. Dickinson, F. Caccavo Jr., B.H. Olesen, Z. Lewandowski, Appl. Environ. Microbiol. 63 (7) (1997) 2502.
[31] B.H. Olesen, R. Avci, Z. Lewandowski, in: Proceedings of Corrosion 1998, Paper no. 275, NACE, Houston, TX, 1998.
[32] B.H. Olesen, R. Avci, Z. Lewandowski, Corros. Sci. 42 (2) (2000) 211.
[33] X. Shi, R. Avci, Z. Lewandowski, Corros. Sci. 44 (5) (2002) 1027.
[34] D.T. Ruppel, S.C. Dexter, G.W. Luther III, Corrosion 57 (10) (2001) 863.
[35] M. Geiser, R. Avci, Z. Lewandowski, Int. Biodeter. Biodegrad. 49 (2002) 235.
[36] M. Geiser, R. Avci, Z. Lewandowski, in: Proceedings of Corrosion 2001, Paper no. 01257, NACE, Houston, TX, 2001.
[37] D. Walsh, D. Pope, M. Danford, T. Huff, J. Min. Met. Mater. Soc. 45 (9) (1993) 22.
[38] M. Da Cunha Belo, B. Rondot, C. Compere, M.F. Montemor, A.M.P. Simoes, M.G.S. Ferreira, Corros. Sci. 40 (2/3) (1998) 481.
[39] D. Briggs, A. Brown, J.C. Vickerman, Handbook of Static Secondary Ion Mass Spectrometry, John Wiley & Sons, New York, 1990.
[40] N.M. Reed, J.C. Vickerman, Static SIMS—surface analysis of inorganic materials, in: D. Briggs, M.P. Seah (Eds.), Practical Surface Analysis, second ed., Ion and Neutral Spectroscopy, vol. 2, John Wiley & Sons, New York, 1996, pp. 303–366.
[41] S.S. Cristy, Secondary ion mass spectrometry, in: C.M. Barshick, D.C. Duckworth, D.H. Smith (Eds.), Inorganic Mass Spectrometry: Fundamentals and Applications, Marcel Dekker, New York, 2000, pp. 159–221.
[42] X. Shi, R. Avci, Z. Lewandowski, in: Proceedings of Corrosion 2002, Paper no. 02256, NACE, Denver, CO, 2002.